



The effects of bifunctional linker and reflux time on the surface properties and photocatalytic activity of CdTe quantum dots decorated KTaO₃ composite photocatalysts

Beata Bajorowicz ^{a,*}, Joanna Nadolna ^a, Wojciech Lisowski ^b, Tomasz Klimczuk ^c, Adriana Zaleska-Medynska ^a

^a Department of Environmental Technology, Faculty of Chemistry, University of Gdańsk, Wita Stwosza 63, 80-308, Gdańsk, Poland

^b Institute of Physical Chemistry, Polish Academy of Sciences, Kasprzaka 44/52, 01-224 Warsaw, Poland

^c Department of Solid State Physics, Faculty of Applied Physics and Mathematics, Gdańsk University of Technology, Narutowicza 11/12, 80-233 Gdańsk, Poland

ARTICLE INFO

Article history:

Received 2 June 2016

Received in revised form

12 September 2016

Accepted 8 October 2016

Available online 13 October 2016

Keywords:

CdTe quantum dots

Photocatalysis

Perovskite-type KTaO₃

Bifunctional linker

ABSTRACT

Novel CdTe-KTaO₃ composite photocatalysts were successfully synthesized by using thioglycolic acid (TGA) or 3-mercaptopropionic acid (MPA) as linker molecules which facilitated attachment of CdTe quantum dots to the surface of KTaO₃ nanocubes. The as-prepared photocatalysts were characterized by UV-vis diffuse reflectance spectroscopy (DRS), X-ray diffraction (XRD), scanning electron microscopy (SEM), transmission electron microscopy (TEM) with energy dispersive X-ray analysis (EDX), Fourier transform infrared spectroscopy (FT-IR), Brunauer–Emmett–Teller (BET) specific surface area, X-ray photoelectron spectroscopy (XPS) and photoluminescence (PL) emission spectroscopy. The obtained CdTe-decorated KTaO₃ composites showed greatly improved photocatalytic performance for degradation of toluene in the gas phase under LEDs light irradiation ($\lambda_{\text{max}} = 415 \text{ nm}$) over pristine KTaO₃. TGA-functionalized CdTe-KTaO₃ composites exhibited higher photocatalytic activity as compared with MPA-capped CdTe-KTaO₃ hybrids which can be ascribed to the shorter chain length of TGA molecule as compared with MPA linker and therefore faster electron transfer from TGA-CdTe nanodots to perovskite-type potassium tantalate. The significance of quantum size effect of CdTe QDs for enhancing photocatalytic performance of CdTeQDs-decorated KTaO₃ was also discussed.

© 2016 Elsevier B.V. All rights reserved.

1. Introduction

In recent years, the perovskite-type oxides containing transition-metal ions (such as Ti, Nb, Ta) have been attracting considerable attention due to their interesting properties and potential photocatalytic applications [1–3]. Tantalum-based materials can be particularly promising photocatalysts because their conduction bands consist Ta 5d orbitals located at the more negative positions than the one of niobates (Nb 4d) or titanates (Ti 3d) [4]. Therefore, semiconductor tantalates were reported as efficient photocatalysts for both degradation of organic pollutants and water splitting to hydrogen energy [2,5,6]. However, bare tantalates such as KTaO₃ and NaTaO₃ can only be excited by UV

light as a result of their wide intrinsic band gap. Various strategies have been adopted for improving the visible light efficiency of wide band gap semiconductors, including doping of heteroatoms, coating of metals, utilizing excitation of surface plasmons by semiconductor particles, absorption of organic or inorganic dyes and quantum dot-sensitization [7–12].

Among these approaches, quantum dot-sensitization has drawn significant attention due to high charge separation efficiency and quantum confinement effects of QDs [10,13]. Xia et al. designed a new class of CQDs/BiOX hybrids with enhanced photocatalytic activity which was ascribed to the better optical absorption and high separation efficiency of the photogenerated electron-hole pairs induced by carbon quantum dots [14]. Di et al. synthesized CQDs/BiOI microsphere with improved photocatalytic efficiency which was assigned to the excellent contact interface, the effective separation of charge carriers and the CQDs acted as photocatalytic reaction centers [15]. It is worth to note that the light absorp-

* Corresponding author.

E-mail address: beatabajorowicz@gmail.com (B. Bajorowicz).

tion range of quantum dots can be easily tuned by adjusting their sizes due to unique size and shape dependent optical properties that they exhibit [16]. Therefore, these semiconductor nanocrystals are able to effectively utilize the visible light but it is necessary to provide strong coupling of QDs and semiconductor photocatalyst. There are various methods to attach QDs to the surface of semiconductor, including direct adsorption [17,18], combination of previously prepared QDs with precursors of semiconductor [19–22] or mixing of semiconductor with precursors of QDs [23] as well as linker-assisted attachment rout [24]. Among these, bifunctional linker-assisted anchoring of QDs to surface of semiconductor substrate is an appealing strategy to obtain stable QDs-semiconductor interface as well as enable maximal control over the size and size distribution of adsorbed QDs [25]. Qian et al. [26] prepared CdS QDs-TiO₂ photocatalysts using direct deposition or bifunctional linker-assisted method. It was observed that strong coupling between CdS and TiO₂ prepared by bifunctional molecule could promote the photocatalytic activity and stability of the composites [26]. In other study, Györi et al. [27] showed that PbSe quantum dots attached to the surface of the anatase TiO₂ nanowires by thioglycolic acid linker are efficient photosensitizers for the visible spectral range. In the presence of TiO₂ decorated with PbSe QDs of 2.5 nm mean diameter 90% of the initial concentration of methyl orange was degraded after 6 h of visible light irradiation [27]. It is also interesting to note that the influence of various types of bifunctional linker used to prepare QDs-semiconductor system was studied for solar cells applications. It was shown that type of linker plays an important role in the electron transfer and overall efficiency of solar cells [28,29]. However, to the best of our knowledge there is no report about influence of various types of bifunctional linker on QDs-decorated material hybrids in regard to their photocatalytic activity.

Cadmium telluride with a band gap of 1.54 eV is a direct band gap semiconductor with a high optical absorption coefficient. Thiol-capped CdTe quantum dots are the most successful example of the colloidal nanocrystals directly synthesized in aqueous solution [30]. The most often used ligands for preparation of highly stable and luminescent CdTe QDs are: 3-mercaptopropionic acid (MPA), thioglycolic acid (TGA), mercaptoethanol, thioglycerol (TG), L-cysteine, mercaptoethanol and cysteamine [30,31]. Li and co-workers [32] synthesized mercapto-capped CdTe QDs-modified TiO₂ photocatalysts which showed enhanced photocatalytic activity as compared with controlled TiO₂ and P25 for malachite green degradation under halogen-tungsten lamp irradiation. It was attributed to the strong absorption and low recombination rate of the electron hole-pairs in CdTe-TiO₂ heterojunction [32]. In other study, Wang et al. [33] synthesized CdTe QDs encapsulated in Zeolite Y nanocomposites in an aqueous medium. CdTe/Y samples exhibited good photocatalytic activity for the decolorization of methyl blue under UV-light irradiation – 87.7% degradation rate was achieved within 30 min [33]. However, apart from above reports, semiconductor photocatalysts modified with CdTe quantum dots were not well reported and investigated.

In this study, we designed and synthesized novel photocatalysts based on KTaO₃ and functionalized CdTe quantum dots with various sizes. The influence of type of bifunctional linker molecule and reflux time of QDs on the absorption and luminescent properties, morphology, surface area, structure and photocatalytic activity of obtained MPA- or TGA-modified CdTe-KTaO₃ photocatalysts were systematically investigated. The photocatalytic efficiency and stability of the as-prepared composites were evaluated in toluene degradation in the gas phase under LEDs light irradiation ($\lambda_{\text{max}} = 415 \text{ nm}$). A possible mechanism related to photogenerated electron transfer between functionalized quantum dots of different sizes and KTaO₃ was proposed and discussed in detail.

2. Experimental

2.1. Materials and instruments

Tantalum (V) oxide (>99% Aldrich, Poznan, Poland) and potassium hydroxide (Chempur, pure p.a.) were used as precursors for the preparation of KTaO₃. Cadmium chloride (CdCl₂, 99%), sodium tellurite (Na₂TeO₃, 99%), L-Ascorbic acid (C₆H₈O₆, reagent grade), 3-mercaptopropionic acid (MPA, 99%), thioglycolic acid (TGA, 99%), ethanol, polyethylene glycol 400 (PEG-400), sodium hydroxide were purchased from POCH S.A. (Gliwice, Poland). Deionized water was used for all reactions and treatment processes. All chemicals were of analytical reagent grade and were used as received without further purification.

Nitrogen adsorption-desorption isotherms at -196°C were measured using a Micromeritics Gemini V (model 2365) physisorption analyzer (Micromeritics Instrument, Norcross, GA, USA). Specific surface areas were calculated following typical Brunauer–Emmett–Teller (BET) method using the adsorption data in the relative pressure (p/p_0) range from 0.05 to 0.3. Prior to adsorption measurements the samples were degassed under vacuum at 200°C for 2 h. Diffuse reflectance spectra (DRS) of the synthesized materials were characterized using the Thermo Scientific Evolution 220 UV-vis spectrophotometer (Thermo Scientific, Waltham, MA, USA) equipped with ISA-220 integrating sphere accessory. The UV-vis DRS spectra were recorded in the range of 200–800 nm using a barium sulfate reference. Powder X-ray diffraction (PXRD, Philips/PANalytical X'Pert Pro MPD diffractometer, Cu K α radiation $\lambda = 1.5418 \text{ \AA}$) was used to determine the phase composition and calculate lattice parameters of polycrystalline samples. The morphology of the semiconductor composites was investigated by scanning electron microscopy (SEM) technique using Hitachi Microscope TM-1000 under high vacuum with accelerating voltage 15 kV as well as transmission electron microscopy (STEM-EDX, FEI Europe, model TecnaiF20 X-Twin) and selected area electron diffraction (SAED). X-ray photoelectron spectroscopic (XPS) measurements were performed using the PHI 5000 VersaProbe (ULVAC-PHI) spectrometer with monochromatic Al K α radiation ($h\nu = 1486.6 \text{ eV}$) from an X-ray source operating at $100 \mu\text{m}$ spot size, 25 W and 15 kV. The high-resolution (HR) XPS spectra were collected with the hemispherical analyzer at the pass energy of 23.5 eV, the energy step size of 0.1 eV and the photo-electron take off angle 45° with respect to the surface plane. The CasaXPS software (version 2.3.16) was used to evaluate the XPS data. The binding energy (BE) scale of all detected spectra was referenced by setting the BE of the aliphatic carbon peak (C-C) signal to 285.0 eV. FT-IR spectra were carried out on a Bruker model IFS66 FTIR spectrometer using potassium bromide discs. The photoluminescence (PL) emission spectra were recorded using a Perkin-Elmer Luminescence Spectrometer LS 50B. The samples were excited with 325 nm and 415 nm wavelength light at room temperature and the emission was scanned between 350 and 700 nm.

2.2. Preparation of KTaO₃

The KTaO₃ semiconductor was prepared by the hydrothermal method based on our previous work with a little modification [2]. In a typical procedure for the preparation of potassium tantalate, KOH (30 g) was dissolved in deionized water (60 mL), then Ta₂O₅ (11 g) and PEG-400 (1 mL) were added. This mixture was stirred for 1 h before it was transferred into a Teflon-lined stainless steel autoclave. The autoclave was sealed and got heated at 200°C for 24 h. After cooling naturally to room temperature, the resulting powder was washed several times by centrifugation with distilled

water and ethanol respectively and dried in an oven at 70 °C for 8 h. Finally, some white powder was obtained.

2.3. Preparation of MPA- and TGA-coated CdTe QDs

CdTe QDs were synthesized via a method similar to that described by Xie et al. [34] with minor modifications. Briefly, CdCl₂ (2 mmol) was dissolved in 100 mL of deionized water in a 250 mL three-neck flask, then TGA or MPA (0.2 mL) was added. Under magnetic stirring, the pH of the mixture was adjusted to 10.5 by using the dropwise addition of NaOH solution (1 mol/L). The above solution was then rested for several minutes, 5 mL of 0.1 mol/L C₆H₈O₆ solution and 0.1 mmol Na₂TeO₃ were added successively under magnetic stirring and the pH value of the resulting solution was readjusted to 10.5. The resulting solution mixture was then heated to 100 °C and refluxed under open-air conditions for 0.5, 2, 5, 8 h, respectively.

2.4. Preparation of CdTe quantum dot-sensitized KTaO₃ composites

CdTe QDs-KTaO₃ photocatalysts were synthesized by linker-assisted attachment method. As wide band gap semiconductor such as KTaO₃ has a strong affinity for the carboxylate group of the linker molecules, bifunctional molecules (HOOC-R-SH) with carboxylate and thiol functional groups were used to enable the binding of CdTe QDs to KTaO₃. The mercapto group was conjugated with Cd²⁺ ion on the surface of CdTe QDs, while the carboxylate group was ionized in the water to make CdTe QDs water soluble. The obtained nanocrystals were adsorbed to the KTaO₃ by carboxylate group. Typically, 50 mL of solution containing the CdTe quantum dots was ultrasonicated for 30 min to make CdTe QDs totally dispersed. The as-prepared KTaO₃ powder (1.0 g) was added into the above solution and stirred for 24 h. Finally, the samples were dried at 70 °C for 12 h.

2.5. Measurement of photocatalytic activity

The photocatalytic activity of the prepared semiconductors and their nanocomposite powders was also determined in the toluene degradation process. Toluene, an important volatile organic compound (VOC), was used as a model air contaminant. The photocatalysts activity tests were carried out in the flat stainless steel reactor ($V = 30 \text{ cm}^3$) equipped with a quartz window, two valves and a septa. As an irradiation source there was used an array of 25 LEDs ($\lambda_{\text{max}} = 415 \text{ nm}$). In a typical measurement the semiconductor powder (about 0.1 g) was suspended in a small amount of water and loaded as a thick film on a glass plate (3 cm × 3 cm) using painting technique. The obtained semiconductors coated support was dried and then placed at the bottom side of the photoreactor followed by closing the reactor with a quartz window. The gaseous mixture from a cylinder was passed through the reactor space for 1 min. The concentration of toluene in a gas mixture was about 150 ppm. After closing the valves, the reactor was kept in the dark for 30 min to reach adsorption equilibrium. A reference sample was taken just before starting irradiation. To estimate toluene concentration the samples were taken every 10 min during 60 min of irradiation. The photocatalytic stability was estimated in four subsequent cycles of toluene degradation. The analysis of toluene concentration in the gas phase was carried out using a Perkin Elmer Clarus 500 GC (Perkin Elmer, Waltham, MA, USA) equipped with a 30 m × 0.25 mm Elite-5 MS capillary column (0.25 μm film thickness) and a flame ionization detector (FID). The samples (200 μL) were injected by using a gas-tight syringe. Helium was used as a carrier gas at a flow rate of 1 mL/min. In addition, to investigate toluene loss due to adsorption at the photocatalyst surface and direct photolysis,

the control experiments were conducted in the presence of photocatalyst in the dark condition and under visible light without photocatalyst, respectively. The toluene concentration decreased in the dark experiment of about 8% after 60 min. The loss of pollutant concentration was negligible during direct irradiation in the absence of photocatalyst.

3. Results and discussion

3.1. Optical properties and BET surface area

Fig. 1. shows the absorption spectra of the pure KTaO₃, MPA-CdTe and TGA-CdTe nanodots as well as KTaO₃ nanocubes modified with MPA- or TGA-capped CdTe quantum dots with various sizes. The absorption edge of pure KTaO₃ semiconductors is approximately 360 nm, which indicates that it absorbs the ultraviolet light and coincides with previous reports [2,35]. The introduction of CdTe QDs into KTaO₃ nanocubes significantly extends the absorption spectrum of the potassium tantalate into the visible region, due to the photosensitizing effect of the incorporated CdTe QDs [10]. In the case of MPA-CdTe-KTaO₃ composites, one can observe the red-shift with increasing reflux time of CdTe QDs which is a clear evidence of nanocrystals growth (**Fig. 1a**). For TGA-CdTe-KTaO₃ samples it can also be seen that absorbance peaks are shifted to longer wavelengths as compared with pristine KTaO₃. However, it is worth noting that TGA-CdTe-KTaO₃ samples that were refluxed for 0.5 h and 2 h exhibited very comparable absorbance. The absorption properties were also very similar for TGA-capped composites refluxed for 5 and 8 h (**Fig. 1b**). All these results confirm that sensitization of KTaO₃ with CdTe QDs can improve the absorption of visible light effectively which could be beneficial for photocatalytic degradation of organic pollutants.

The size of CdTe QDs was changed by varying the reflux time (0.5, 2, 5, 8 h) and is shown in **Table 1**. The average diameters of CdTe nanodots were calculated according to empirical equation proposed by Yu et al. [36] as follows:

$$D = (9.8127 \times 10^{-7})\lambda^3 - (1.7147 \times 10^{-3})\lambda^2 + (1.0064)\lambda - (194.84),$$

where D is the average diameter of the quantum dots (nm); λ is the wavelength corresponding to maximum absorbance.

The Kubelka–Munk method was used to estimate the band gaps of the obtained samples. The insets of **Fig. 1c,d** depict the plots of transformed Kubelka–Munk function as a function of photoenergy. The estimated band gap energies are summarized in **Table 1**. It should be noted that the band gaps of QDs decreased with increasing their sizes which can be ascribed to the quantum confinement effects of CdTe nanocrystals [37].

The BET surface areas of KTaO₃ and KTaO₃-CdTe QDs composites prepared in the presence of MPA or TGA are summarized in **Table 1**. The surface areas of as-prepared samples fluctuated from 0.1 to 1.64 m²/g and were dependent on reflux time of CdTe QDs as well as type of capping agent (MPA or TGA). The pristine KTaO₃ had BET surface area about 1.64 m²/g which coincide with our previous study [35]. MPA- or TGA-capped CdTe quantum dots modified KTaO₃ revealed reduced surface area as compared with pristine KTaO₃. Shrunken surface area of TGA/MPA-CdTe-KTaO₃ composites could result from aggregation of KTaO₃ crystals observed by SEM (data not shown) during modification by CdTe quantum dots due to the presence of bifunctional linker molecules. Moreover, it could be seen that all composite samples covered with TGA presented higher surface area than samples with MPA refluxed for the same amount of time. The highest BET surface area among all CdTe-KTaO₃ composites was observed for TGA-CdTe sample containing nanodots refluxed for 2 h while the lowest surface area was shown by MPA-CdTe-KTaO₃ sample containing QDs refluxed

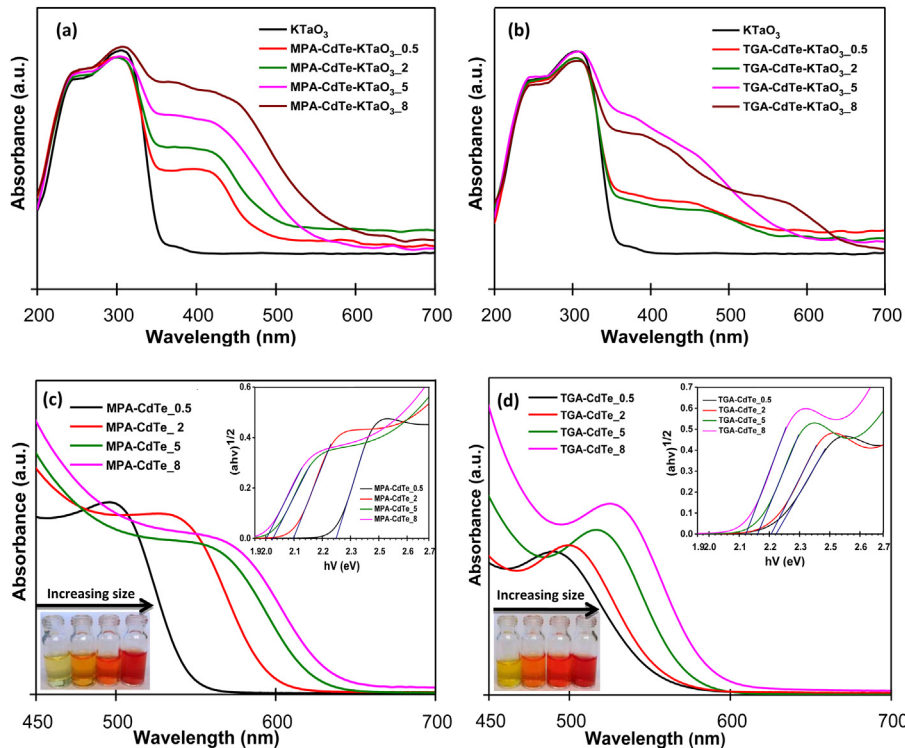


Fig. 1. The UV-vis diffuse reflectance spectra of (a) MPA-functionalized CdTe-KTaO₃ composites, (b) TGA-functionalized CdTe-KTaO₃, (c) MPA-CdTe QDs, (d) TGA-CdTe QDs. Plots of the transformed Kubelka–Munk function vs. photon energy of obtained QDs and images of QDs aqueous suspensions have been shown in insets.

Table 1

Sample label, preparation conditions and selected properties of KTaO₃ modified by functionalized CdTe QDs.

Sample label	Type of surface ligand	Reflux time of QDs (h)	Average size of QDs (nm)	Band gap of QDs (eV)	BET surface area (m ² /g)
KTaO ₃	–	–	–	–	1.64
MPA-CdTe-KTaO ₃ -0.5	MPA	0.5	2.23	2.27	0.14
MPA-CdTe-KTaO ₃ -2	MPA	2	2.95	2.08	0.16
MPA-CdTe-KTaO ₃ -5	MPA	5	3.28	1.98	0.13
MPA-CdTe-KTaO ₃ -8	MPA	8	3.35	1.95	0.25
TGA-CdTe-KTaO ₃ -0.5	TGA	0.5	2.04	2.24	0.15
TGA-CdTe-KTaO ₃ -2	TGA	2	2.32	2.21	0.90
TGA-CdTe-KTaO ₃ -5	TGA	5	2.75	2.16	0.19
TGA-CdTe-KTaO ₃ -8	TGA	8	2.90	2.11	0.36

for 5 h. It has been widely recognized that a higher BET surface area could enable absorption of more active species and reactants on their surface and, thus, resulted in higher photocatalytic activity. However, in our study, the modification of KTaO₃ with CdTe QDs caused the reduction of BET surface area which could indicate that the higher surface area is probably not the major factor that leads to the enhanced photocatalytic performance of CdTe-KTaO₃ nanocomposites. A similar observation was presented by Chen et al. [38]. They reported that the anchoring of Cu_xO or Fe_xO quantum dots on TiO₂ decreased the specific surface area of TiO₂ but did not cause its lower photocatalytic activity [38]. In other study, Di and co-workers [39] reported that the BET surface area of the C QDs modified BiOCl composites was smaller than the one of pristine BiOCl nanosheets but the specific surface area was not the main factor responsible for the higher photocatalytic activity of CQDs-BiOCl materials [39].

3.2. Morphology

The SEM, TEM and HRTEM measurements were performed to characterize the morphology and microstructure of the as-prepared samples. Fig. 2a presents SEM image of pristine potassium

tantalate which exhibits cube-like shape with diameter of about 0.1–1.5 μm. Fig. 2b displays the TEM image of well-developed cubic crystal of KTaO₃. Fig. 2c,d shows TEM images of CdTe-KTaO₃ composites prepared using MPA or TGA as linker molecules that attach the quantum dots to the surface of the KTaO₃. It was clearly observed that the CdTe QDs were combined with KTaO₃ and did not affect the cubes of the potassium tantalate. Moreover, this intimate contacted interface between potassium tantalate and cadmium telluride nanodots may play an important role for accelerating the separation of the photogenerated charge carriers [40].

Fig. 2e,g displays the highly magnified TEM image of the MPA-CdTe-KTaO₃-2 and TGA-CdTe-KTaO₃-0.5 composites, where CdTe QDs were loaded on the surface of the KTaO₃. As can be seen from these figures, the average size of the CdTe nanodots is about 3 nm which is quite close to that calculated from the UV-vis absorption spectra. However, it can be also observed that some MPA-CdTe QDs tended to agglomerate into larger particles on the surface of potassium tantalate cubes (Fig. 2f).

As observed from HRTEM image, the lattice spacings of 0.285 nm belong to the (110) plane of the cubic perovskite phase of KTaO₃, suggesting that obtained potassium tantalate was well crystallized [41,42]. Meanwhile, the well-resolved lattice fringes of the small

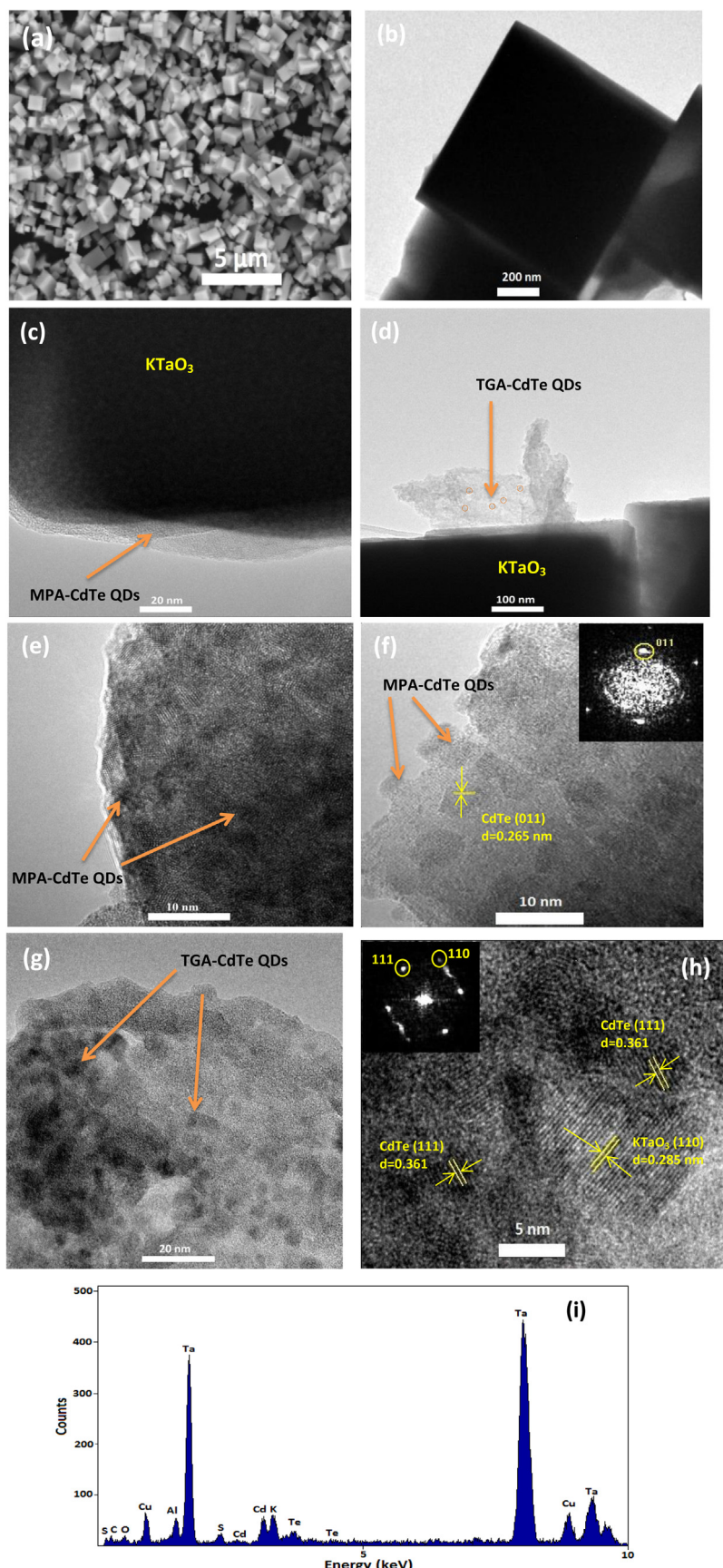


Fig. 2. (a) SEM image of KTaO₃; TEM images of (b) pristine KTaO₃, (c,e) MPA-CdTe-KTaO₃_{0.5} composites, (d,g) TGA-CdTe-KTaO₃_{0.5} composites, HRTEM images of (f) MPA-CdTe-KTaO₃₂ composites and (h) TGA-CdTe-KTaO₃₂ composites; (i) EDS spectrum of TGA-CdTe-KTaO₃_{0.5} photocatalyst.

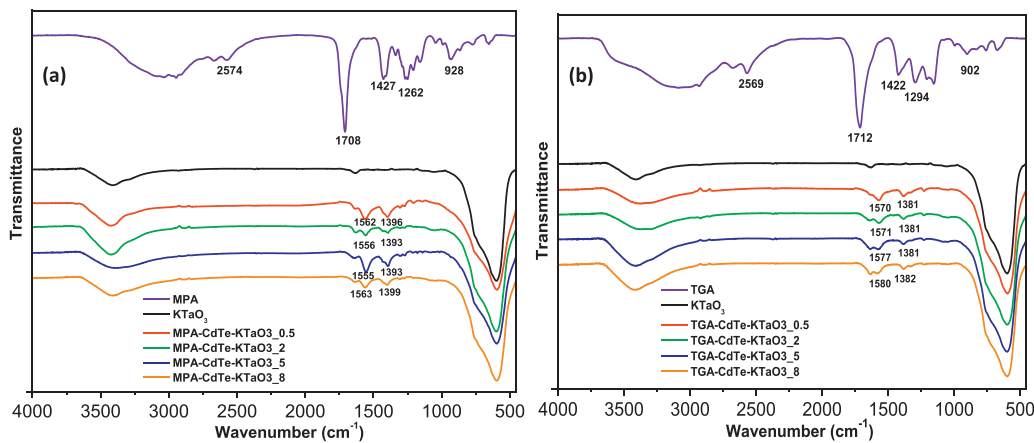


Fig. 3. FT-IR spectra of (a) MPA, pristine KTaO₃ and MPA-CdTe-KTaO₃ composites, (b) TGA, pristine KTaO₃ and TGA-CdTe-KTaO₃ samples.

crystallites located on the surface of KTaO₃ sample are detected to be 0.361 nm and 0.265 nm, corresponding to (111) and (011) planes of CdTe (JCPDS 65-1046), respectively (yellow lines and arrows in Fig. 2f,h) [43,44]. Therefore, these results confirm that CdTe nanodots have been successfully combined with the KTaO₃ nanocubes and the heterojunctions in the fabricated composites were formed.

The elemental composition of the final products was also analyzed by the energy dispersive spectrometry (EDS), and the results are displayed in Fig. 2i. The EDS patterns of the TGA-CdTe-KTaO₃ composite indicated the presence of K, Ta, O diffraction peaks coming from KTaO₃ as well as Cd and Te peaks corresponding to CdTe quantum dots which confirmed that the obtained samples were composed of KTaO₃ and CdTe. Moreover, among these elements, S, C and O were from the bifunctional surface ligand. In EDX spectra, Al and Cu peaks came from sample holder and copper grid, respectively.

3.3. FT-IR analysis

Fourier transform infrared spectroscopy (FT-IR) was used to determine whether the –COOH group of bifunctional ligands (MPA and TGA) chemically adsorbed to the surface of KTaO₃ and whether the –SH group of linker molecules was chemically bonded to the CdTe quantum dots surface. FT-IR spectra of bare KTaO₃, TGA- and MPA-capped CdTe QDs-KTaO₃ composites as well as free MPA and TGA are shown in Fig. 3. The 1427 cm^{-1} and 1422 cm^{-1} symmetric C–O stretching (CO_2H) mode as well as 1262 cm^{-1} and 1294 cm^{-1} C–O–H bending ($\delta(\text{CsOsH})$) mode of the free MPA and free TGA, respectively, were greatly diminished or not present in the spectra of MPA-CdTe-KTaO₃ and TGA-CdTe-KTaO₃ composites which indicates that bifunctional acids bind chemically to the potassium tantalate surface through the carboxylic acid groups [26,45]. Moreover, it can be observed that there is shift of the asymmetric stretching vibration of carboxyl group from 1708 cm^{-1} (free MPA) and 1712 cm^{-1} (free TGA) to ~1560 cm^{-1} (MPA-modified composites) and ~1570 (TGA-modified composites) implying that the carboxyl group turned into its anion and led to an intensive symmetric vibration of the carboxyl anion at ~1396 cm^{-1} and ~1381 cm^{-1} for MPA-CdTe-KTaO₃ and TGA-CdTe-KTaO₃ samples, respectively. It is an additional proof of the chemical attachment of the MPA or TGA to the KTaO₃ surface through the carboxylic group [26,46,47].

The weak peaks in the region of 2940–2850 cm^{-1} correspond to the $\nu(\text{C–H})$ vibrational modes of the –CH₂– of the bifunctional acids (MPA or TGA) [48]. Pristine KTaO₃ as well as all CdTe-KTaO₃ samples revealed the broad and intensive bands in the region from 850 to 500 cm^{-1} which correspond to Ta–O bonding [49]. All the samples also presented a strong band located at approximately

3400 cm^{-1} which can be ascribed to the stretching vibration of hydroxyl groups and water molecules adsorbed on the surface of photocatalysts [32,50].

In addition, in the IR spectra of free bifunctional acids the appearance of peaks at 2574 cm^{-1} (MPA) and 2569 cm^{-1} (TGA) as well as 928 cm^{-1} (MPA) and 902 cm^{-1} (TGA) could be assigned to the S–H stretching as well as bending modes, respectively [48]. However, there are no characteristic peaks of the mercapto group in the TGA- and MPA-capped CdTe-KTaO₃ composites which indicates the cleavage of the S–H bond and the formation of a new S–Cd bond between TGA or MPA and CdTe QDs [47,51,52]. All of these results confirm that CdTe nanodots can be successfully bonded to the surface of KTaO₃ using 3-mercaptopropanoic acid or thioglycolic acid as linker molecules.

3.4. XRD analysis

The room temperature powder X-ray diffraction (PXRD) pattern for the KTaO₃ sample with a successful profile fit (Le Bail method) of the data to the perovskite structure type (*Pm-3m*), is shown in Fig. 4. The high purity of KTaO₃ sample is confirmed by the excellent quality of the refinement and the absence of addi-

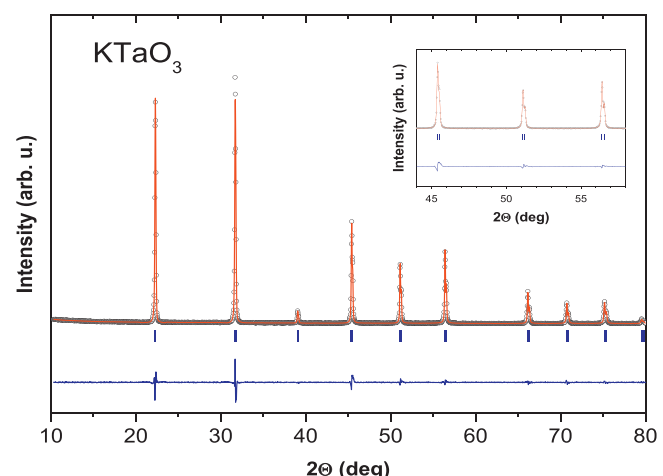


Fig. 4. (a) The Le Bail refinement of room temperature powder x-ray diffraction data for KTaO₃. Black points – observed intensities (I_{obs}), red line – calculated intensities (I_{calc}), blue line – $I_{\text{obs}} - I_{\text{calc}}$. The blue tick marks correspond to the expected positions of Bragg reflections for the used model. An inset shows the excellent quality of refinement. Figures of merit: $R_p = 7.10$, $Rwp = 9.33$, $Rexp = 6.43$, $\chi^2 = 2.11$. (For interpretation of the references to colour in this figure legend, the reader is referred to the web version of this article.)

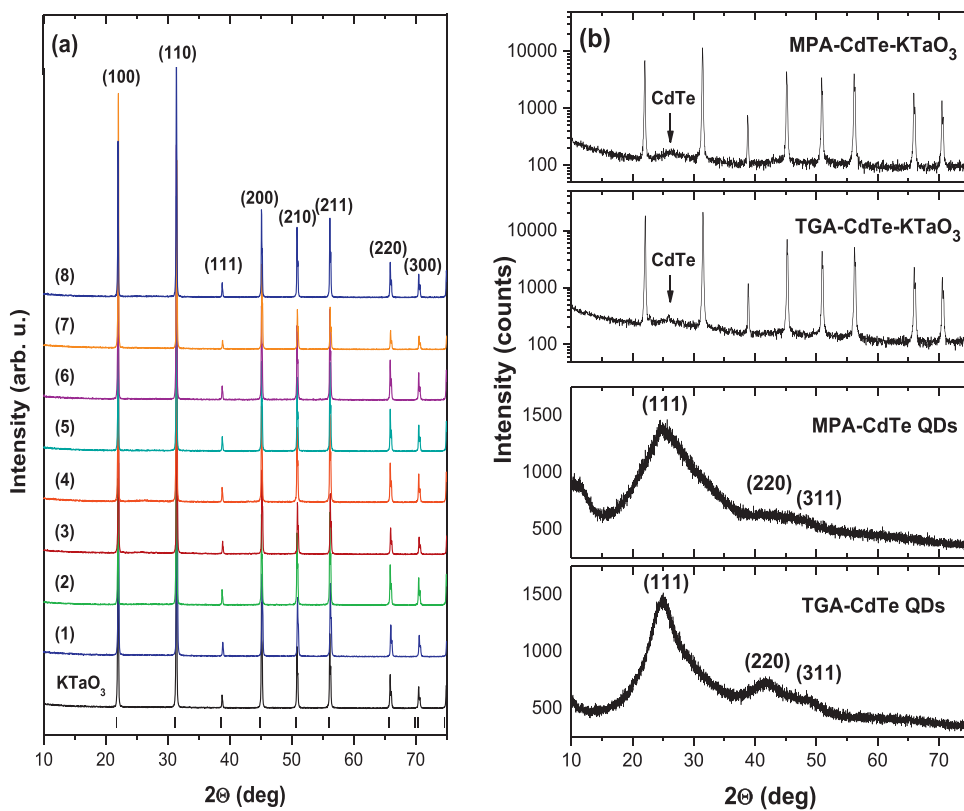


Fig. 5. (a) X-ray diffraction patterns of as-prepared KTaO₃ and (1–4) MPA-CdTe-KTaO₃ composites refluxed for 0.5, 2, 5, 8 h, respectively and (5–8) TGA-CdTe-KTaO₃ composites containing QDs refluxed for 0.5, 2, 5, 8 h, respectively; (b) XRD patterns (X-ray intensities were measured in counts) of MPA-CdTe-KTaO₃.2 composite, TGA-CdTe-KTaO₃.0.5 composite, MPA-CdTe.2 QDs and TGA-CdTe.0.5 QDs.

tional reflections in the pattern. The estimated lattice parameter $a = 3.9920(1)$ Å is very close to the reported $a = 3.9896(1)$ Å by Tkach et al. [53]. Fig. 5a presents the comparison of the XRD patterns of pristine KTaO₃ with TGA- and MPA-capped CdTe-KTaO₃ composites containing quantum dots refluxed for various time. The diffraction pattern of pristine KTaO₃ shows the distinctive peaks which can be indexed to the (100), (110), (111), (200), (210), (211), (220), (300) and (310) planes of the cubic perovskite structure of potassium tantalate (JCPDS cards 77-0918) [54]. After loading the CdTe quantum dots, the XRD patterns of the CdTe-modified KTaO₃ composites were almost the same as that of pure potassium tantalate which might result from the high dispersion of CdTe quantum dots and the low content of incorporated CdTe QDs [26,55]. It could suggest that loading the CdTe nanocrystals using bifunctional linker coupling method did not destroy the KTaO₃ crystal structure.

Additionally, Fig. 5b. shows XRD patterns (where X-ray intensities were measured in counts) for MPA- and TGA-capped CdTe nanodots as well as XRD patterns for MPA-CdTe-KTaO₃.2 and TGA-CdTe-KTaO₃.0.5 composites. It can be seen from this figure that the X-ray diffraction pattern of bare CdTe nanodots presents broad peaks typical for nanocrystals. The three distinct peaks at 25°, 41° and 49° correspond to (111), (220) and (311) planes of cubic zinc blended structure of CdTe QDs (JCPDS File No.65-1046) [34]. However, the intensity of diffraction peaks of MPA-CdTe nanodots was significantly lower than the peaks intensity of the CdTe nanodots in which TGA was used as a surface ligand. The lower intensity indicates a more amorphous structure of MPA-capped CdTe QDs as compared with TGA-capped nanodots. In the case of MPA-CdTe-KTaO₃.2 and TGA-CdTe-KTaO₃.0.5 samples there are two obvious peaks corresponding to the perovskite KTaO₃ as well as the rather weak and broad peaks centred at 25° which can be indexed to the (111) planes of cubic CdTe quantum dots [56]. The much lower

intensities of CdTe QDs as compared with KTaO₃ could be attributed to their very small size, low content and the presence of amorphous capping ligand (MPA or TGA) surrounding CdTe QDs [56].

3.5. XPS analysis

Table S1 of Supplementary material in the online version at DOI: <http://dx.doi.org/10.1016/j.apcatb.2016.10.027> shows the composition and chemical characters of elements formed in the surface layer of KTaO₃ and KTaO₃ modified by CdTe QDs synthesized using MPA or TGA linker and refluxed under open-air conditions for 0.5, 2, 5, 8 h, respectively. The presented XPS data were obtained after analysis of high-resolution (HR) XPS spectra of Ta4f, K2p, O1s, C1s, S2p, Cd3d and Te3d for all detected elements; tantalum, potassium, oxygen, carbon, sulfur, cadmium and tellurium, respectively. The exemplary HR spectra of elements detected on MPA and TGA samples are shown in Fig. 6. Two presented samples exhibited the best photocatalytic activity among MPA- and TGA-capped CdTe-KTaO₃ composites, respectively.

The Cd3d spectra are partially overlapped by Ta4p_{3/2} XPS signals (Fig. 6a). However, after deconvolution of these spectra two states of Cd3d_{5/2} at binding energy (BE) of 405.0 and 405.7 eV were well distinguished, which can be ascribed to CdTe and CdO, respectively [31,57–59]. The Te3d spectra (Fig. 6b) reveal two states of tellurium at BE of 572.7 and 576.1 eV, respectively, which are characteristic for CdTe and Te-Ox compounds [57,59]. Four states of sulfur, labeled as S1, S2, S3 and S4, were well separated in deconvoluted S2p spectra (Fig. 6c) at BE of 161.3, 162.3, 163.7 and 168.3 eV, respectively. S1 state can be attributed to thiolate [57], S2 to S-CdS_{latt} species [31,57,58], S3 to thiol and sulfide compounds [31,57–59] and S4 to sulfonate surface compounds [59]. The fitted spectra of C1s and K2p are presented in Fig. 6d. Three carbon peaks at BE of 285, 286.2

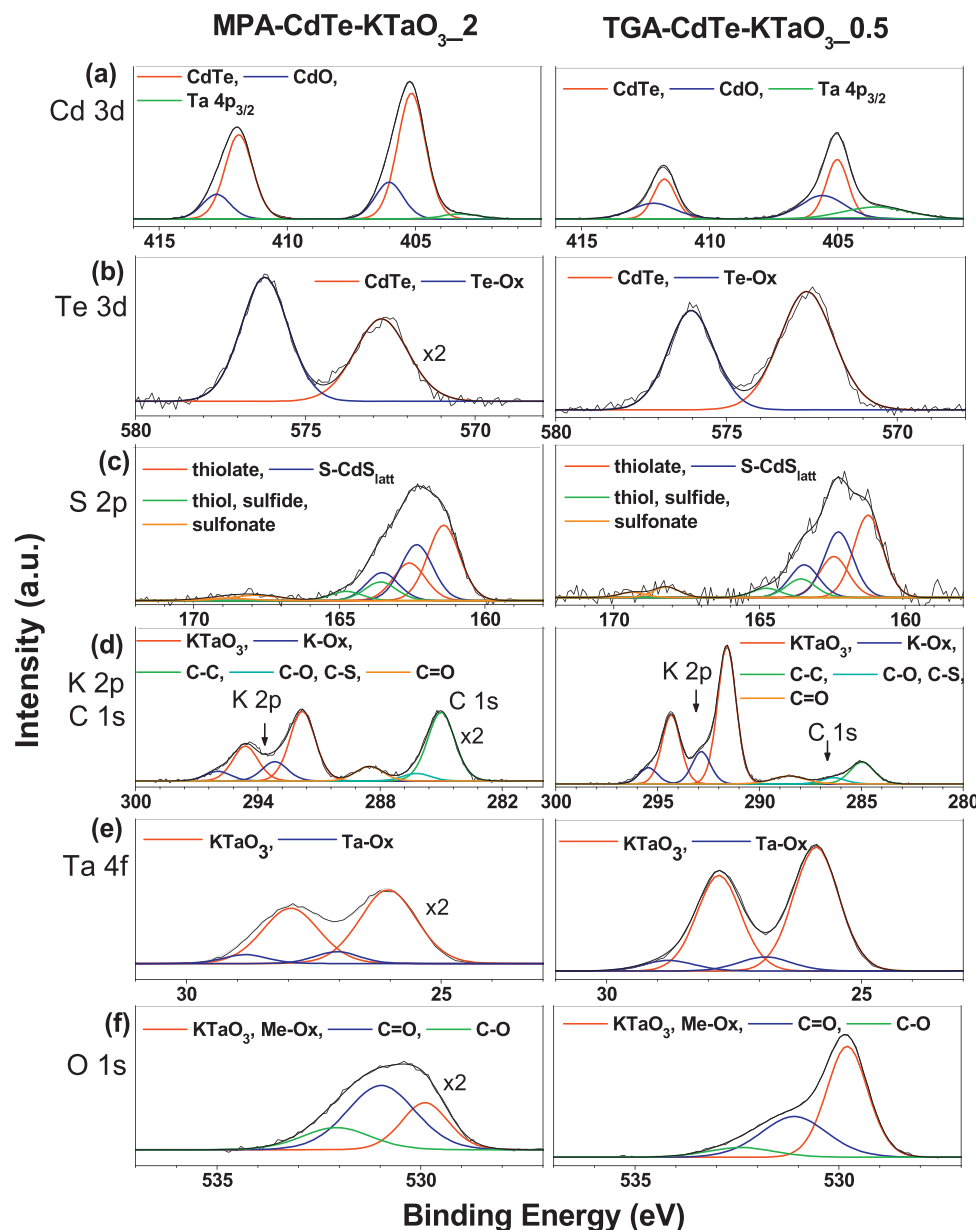


Fig. 6. High-resolution XPS spectra of (a) Cd 3d, (b) Te 3d, (c) S 2p, (d) K 2p and C 1s, (e) Ta 4f, (f) O 1s monitored on MPA-CdTe-KTaO₃.2 (left column) photocatalysts and TGA-CdTe-KTaO₃.0.5 composites (right column).

and 288.5 eV can be assigned to C–C, C–O, C–S and C=O groups, respectively [59]. The K2p line consists of two doublets at BE of K2p_{3/2} at 291.7 and 293.1 eV, respectively. The first doublet, with higher intensity peaks, relates to KTaO₃ crystal lattice [60,61]. The second one can be attributed to K-O complexes [60], which can be formed at the surface during preparation of KTaO₃. The Ta4f spectra (Fig. 6e) exhibit two states at BE of Ta 4f_{7/2} peak at 26 and 28 eV, which can be identified as KTaO₃ and Ta-Ox compounds [60,61]. Finally, deconvolution of O1s spectra (Fig. 6f) reveals three main peaks at BE of 530, 531.2 and 532.4 eV assigned to KTaO₃, Me-Ox (Me = Ta, Cd, Ta, Te), C=O and C–O groups, respectively [59].

Inspection of XPS data, collected in Table S1 of Supplementary material in the online version at DOI: <http://dx.doi.org/10.1016/j.apcatb.2016.10.027>, reveals different elemental composition of MPA- and TGA-modified samples. The total surface content of C, S and Cd on the MPA modified samples was found to be larger than on samples modified by TGA compounds. On the other hand, the rela-

tive surface concentration of K and Ta on MPA-KTaO₃ samples was smaller than on TGA-KTaO₃ samples. As a result the average value of S/K atomic concentration ratio for all MPA- and TGA-modified samples was evaluated to be 1.9 ± 0.7 and 0.5 ± 0.2 , respectively. Similar relationships can be observed for C/K and Cd/K atomic concentration ratios ($C/K(MPA) = 5.5 \pm 2.3$, $C/K(TGA) = 1.0 \pm 0.1$ and $Cd/K(MPA) = 2.1 \pm 0.5$, $Cd/K(TGA) = 0.7 \pm 0.3$). The oxidized forms of Ta, K, C and S become more pronounced at the surface of TGA-modified specimens as the reflux time under open-air conditions increase.

3.6. Photoluminescence properties

Photoluminescence (PL) measurements were used to investigate the excited-state interaction between CdTe quantum dots and KTaO₃ particles. Fig. 7 displays photoluminescence (PL) emission spectra of KTaO₃ and CdTe–KTaO₃ nanocomposites at an excitation

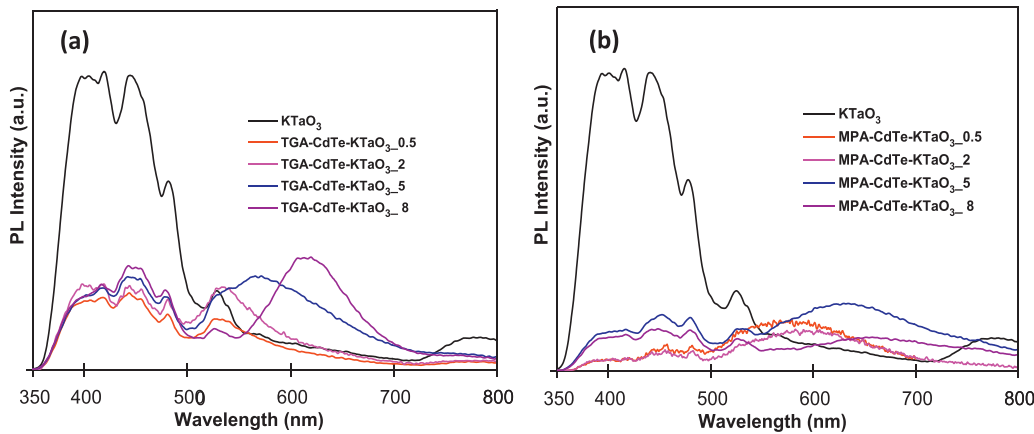


Fig. 7. Photoluminescence emission spectra of (a) TGA-modified CdTe-KTaO₃ composites, (b) MPA-modified CdTe-KTaO₃ composites.

wavelength of 325 nm. Pristine perovskite-type potassium tantalate exhibits blue luminescence (BL) with maximum emission at about 420 nm and 445 nm which can be ascribed to the intrinsic radiative emission associated with the recombination of the electron-hole pairs of a localized exciton in a TaO₆ octahedron [62]. The green luminescence (GL) of KTaO₃ in the region of about 530 nm can be attributed to an extrinsic defect radiation [63]. After loading of CdTe nanodots into potassium tantalate, the intensity of these emission peaks significantly decreased, indicating that the recombination of the photo-excited electrons and holes was effectively restrained by attachment of functionalized CdTe QDs to the surface of KTaO₃. For the CdTe-KTaO₃ composites, the emissions from both the CdTe QDs and KTaO₃ were detected which can confirm successful coupling of nanodots with potassium tantalate. The emissions of QDs corresponds to the remaining luminescence signals after quenching by electron transfer to the KTaO₃ [64,65]. Comparing the changes in PL intensity of all TGA-modified samples (Fig. 7a), it can be easily observed that the luminescence intensity decreased with decreasing reflux time of CdTe QDs while in the case of MPA-functionalized composites (Fig. 7b) this correlation can not be observed. The MPA-CdTe-KTaO₃-2 and TGA-CdTe-KTaO₃-0.5 composites possessed the lowest PL intensity among MPA- and TGA-modified samples, respectively, suggesting the highest separation and transfer efficiency of photogenerated electron-hole pairs. In general, this quenching behavior confirms the excited-state interaction between CdTe quantum dots and potassium tantalate and demonstrates that the most excited electrons were transferred from CdTe to KTaO₃ cubes and therefore can enhance photocatalytic performance of the composites.

3.7. Photocatalytic activity in the gas phase

The effects of type of bifunctional linker and reflux time on the photocatalytic activity were evaluated by degradation of the toluene in the gas phase under LEDs ($\lambda_{\text{max}} = 415 \text{ nm}$) after 60 min in the presence of KTaO₃ modified by CdTe quantum dots synthesized using MPA or TGA linker and refluxed under open-air conditions for 0.5, 2, 5, 8 h, respectively. Toluene, an important volatile organic compound (VOC), was used as a model air contaminant. The efficiency of toluene photodegradation and stability in two subsequent cycles after 60 min in the presence of as-prepared samples is given in Table 2. The kinetics of toluene degradation in the first cycle in the presence of MPA- and TGA-modified composites are shown in Fig. 8. In addition, Fig. 9 presents the recycling of TGA-CdTe-KTaO₃-0.5 sample over four runs. The blank test showed that toluene is only slightly degraded without catalysts (5%), indicating the photolysis of toluene can be ignored. It could be seen

Table 2

Photocatalytic activities of obtained MPA- and TGA-capped samples with various sizes of QDs for toluene photodegradation after 1 h irradiation in two subsequent measurement cycles.

Sample label	Average size of CdTe QDs	Efficiency of toluene photodegradation (%) after 60 min irradiation (LEDs, $\lambda_{\text{max}} = 415 \text{ nm}$)	
		1st cycle	2nd cycle
KTaO ₃	–	47	46
MPA-CdTe-KTaO ₃ -0.5	2.23	60	55
MPA-CdTe-KTaO ₃ -2	2.95	74	71
MPA-CdTe-KTaO ₃ -5	3.28	67	66
MPA-CdTe-KTaO ₃ -8	3.35	53	50
TGA-CdTe-KTaO ₃ -0.5	2.04	87	78
TGA-CdTe-KTaO ₃ -2	2.32	85	80
TGA-CdTe-KTaO ₃ -5	2.75	75	70
TGA-CdTe-KTaO ₃ -8	2.90	81	77

that bare KTaO₃ and all as-prepared CdTe-KTaO₃ composites were photoactive in toluene degradation in the gas phase. Removal efficiency in the presence of pristine KTaO₃ reached about 47% after a 60-min process and photocatalytic activity almost did not change after two subsequent cycles of irradiation. All the obtained CdTe-KTaO₃ composites exhibited higher photocatalytic activity in the gas phase as compared with bare KTaO₃. Moreover, it could be seen that all TGA-capped samples presented higher photoactivity than MPA-capped composites. It may suggest that thioglycolic acid (TGA) is more effective as a linker molecule to combine KTaO₃ with CdTe quantum dots as compared with 3-mercaptopropionic acid (MPA). Furthermore, in comparison with MPA-CdTe-KTaO₃ samples (photocatalytic activity ranging from 53 to 74% in the 1st cycle), TGA-capped composites (photocatalytic activity from 75 to 87%) exhibited lower differences in photodegradation of toluene depending on the reflux time of CdTe QDs. The highest photocatalytic activity (74%) under 415 nm LEDs light after 1 h irradiation among MPA-capped composites was exhibited by MPA-CdTe-KTaO₃-2 sample containing CdTe quantum dots that were refluxed for 2 h at 100 °C. While in the case of TGA-capped composites the highest photocatalytic activity (87%) was observed for TGA-CdTe-KTaO₃-0.5 sample containing CdTe quantum dots that were refluxed for 0.5 h and it was the highest efficiency among all obtained CdTe-KTaO₃ photocatalysts. However, it is worth noting that in the case of TGA-CdTe-KTaO₃-2 composite very high photocatalytic activity in the gas phase (85%) as well as better stability than the one exhibited by TGA-CdTe-KTaO₃-0.5 sample were also observed. It may indicate that optimum reflux time of CdTe QDs for both TGA- and MPA-CdTe-KTaO₃ composites is 2 h. In gen-

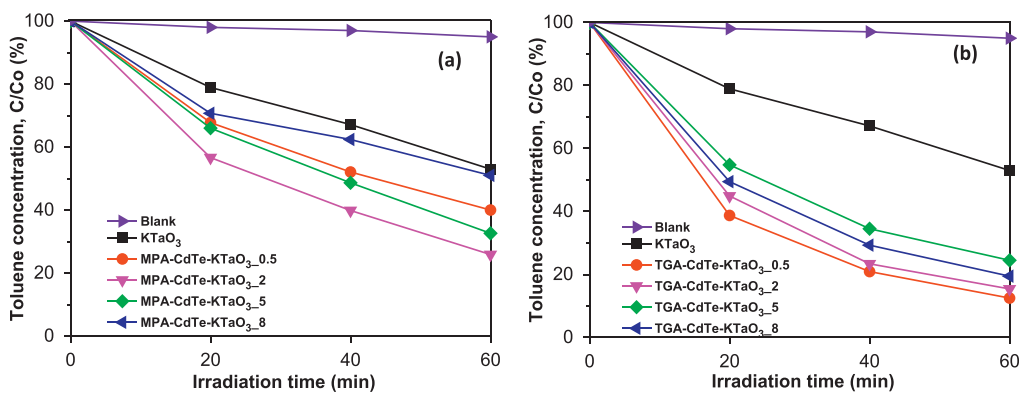


Fig. 8. Efficiency of toluene photodegradation as the function of irradiation time under LEDs irradiation ($\lambda_{\text{max}} = 415 \text{ nm}$) over: (a) MPA-CdTe-KTaO₃ and (b) TGA-CdTe-KTaO₃ composites containing QDs refluxed for 0.5, 2, 5, 8 h, respectively.

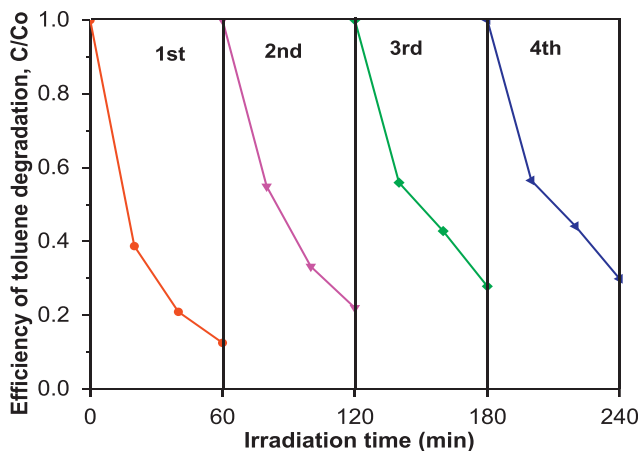


Fig. 9. Recycling performance of TGA-CdTe-KTaO₃-0.5 composite toward toluene photodegradation under LEDs light irradiation ($\lambda_{\text{max}} = 415 \text{ nm}$).

eral, all as-prepared photocatalysts have shown good stability in two subsequent cycles of irradiation. The photocatalytic activity decreased only slightly in the second measurement cycle which suggestss that surface of KTaO₃ may have been blocked by toluene partial decomposition products, as was previously observed for TiO₂-based photocatalysts [66,67]. Furthermore, considering the importance of lifetime of the photocatalyst in practical applications, the reusability of the TGA-CdTe-KTaO₃-0.5 sample after four recycled experiments was also performed. In the presence of TGA-modified-CdTe-KTaO₃-0.5 composite photocatalytic activity decreased from 87% (1st cycle) to 70% (4th cycle) which is probably due to undergoing photocatalytic corrosion of CdTe nanocrystals (Fig. 9). Similar result was obtained for CdSe QDs-modified TiO₂ photocatalysts which exhibited loss in photoactivity after 3 runs because of difficulty in recovering nanoparticles and photocorrosion of CdSe nanodots [68]. Despite this fact, it was shown in this study that incorporation of CdTe QDs into KTaO₃ can significantly enhance photocatalytic activity of KTaO₃ in toluene degradation in the gas phase under visible light.

3.8. Discussion of the photocatalytic mechanism

According to the DRS UV-vis spectra shown in Fig. 1., the incorporation of CdTe QDs into KTaO₃ cubes significantly extended the absorption spectrum of the potassium tantalate into visible region. The enhanced photocatalytic activity can be attributed to the improved optical absorption and the presence of MPA or TGA linker molecules which enabled formation of a stable CdTe-KTaO₃

heterojunction and therefore favored the separation of photo-induced electron-hole pairs in CdTe-KTaO₃ composites (as shown in Fig. 7.). Since the conduction band edge of CdTe is above that of the KTaO₃, the difference between the two conduction band energy levels serves as a driving force for the interparticle electron transfer [69,70].

Under irradiation by LEDs, which emits UV and visible light with maximum at 415 nm, both CdTe quantum dots and KTaO₃ cubes can be excited which result in the formation of corresponding photo-induced carriers (Fig. 11a). Then, photo-induced electron on exterior of CdTe QDs can directly inject into the CB of KTaO₃ due to the presence of bifunctional linker molecules which facilitate intimate contact between quantum dots and potassium tantalate. Meanwhile, holes on the VB of KTaO₃ can be easily transferred to that of CdTe under the potential difference of band energy. Therefore, the photo-generated charges in CdTe and KTaO₃ can be effectively separated. The CB potential of KTaO₃ is negative to the redox potential of O₂•O₂, implying that the photogenerated e⁻ can react with adsorbed O₂ and transform to peroxide radical anions (•O₂⁻). Meanwhile, although •OH radicals cannot be derived by the reaction of the photogenerated h⁺ with OH⁻ or H₂O since the VB potential of CdTe is negative to the redox potentials of H₂O/OH, holes can still directly oxidize toluene. The active oxygen species can cause mineralization and oxidize toluene into CO₂ and H₂O. In order to confirm toluene mineralization ability of photocatalyst, generation of CO₂ during photocatalytic degradation for the TGA-CdTe-KTaO₃-0.5 sample was detected using gas chromatography. It was observed that the amount of CO₂ increased with decreasing toluene concentration indicating the successful mineralization process.

Another evidence for the charge transfer in CdTe-KTaO₃ composites is quenching in the fluorescence of CdTe QDs. Fig. 10 presents fluorescence emission spectra of CdTe quantum dots before and after being anchored into KTaO₃ cubes (recorded using excitation wavelength at 415 nm). The TGA-CdTe and MPA-CdTe nanodots exhibited characteristic emission peaks at 550 nm and 590 nm, respectively. After the nanodots are loaded into the KTaO₃, the composites exhibit almost the same emission peaks as the CdTe QDs, but the emission was greatly diminished. The significant fluorescence quenching can be a signature of electron injection from CdTe nanodots into the KTaO₃ conduction band.

It is also interesting to observe that the photocatalytic activity varies with different-sized (different reflux time) CdTe QDs loaded onto KTaO₃. This result can be explained by the size quantization effect in these nanodots. Controlling particle sizes enables changing the band energies of QDs, and therefore modulating the energy of charge carriers. Bulk CdTe has a band gap of 1.54 eV with conduction band energy at 3.5 eV (vs. vacuum). The band gap energy of CdTe QDs should be higher than 1.54 eV due to the quantum confinement

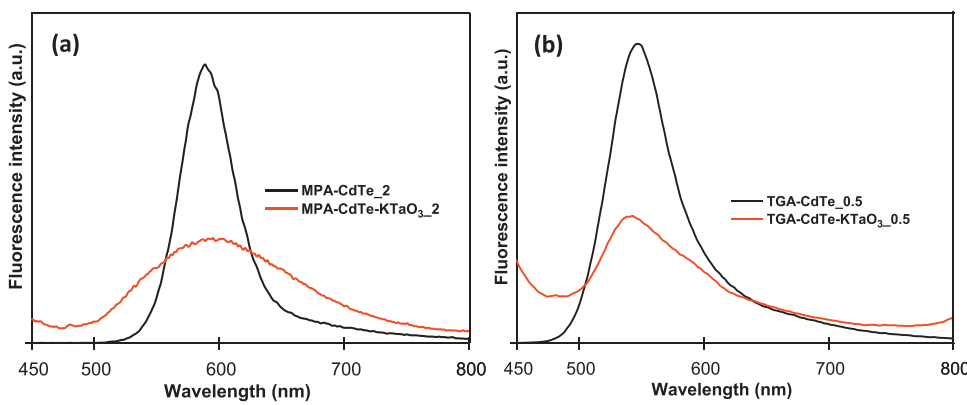


Fig. 10. Fluorescence emission spectra ($\lambda_{\text{exc}} = 415 \text{ nm}$) obtained for (a) MPA-CdTe QDs refluxed for 2 h and MPA-CdTe-KTaO₃_2 composites, (b) TGA-CdTe QDs refluxed for 0.5 h and TGA-CdTe-KTaO₃_0.5 composite.

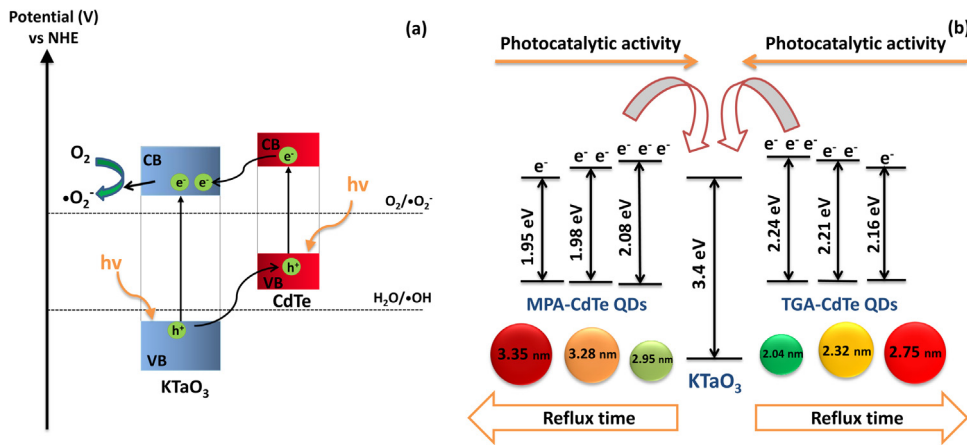


Fig. 11. Proposed photocatalytic mechanism: (a) separation and transfer of photogenerated charge carriers over CdTe-KTaO₃ photocatalysts under LEDs irradiation ($\lambda_{\text{max}} = 415 \text{ nm}$) (b) possible pathway for the electron transfer from various sized CdTe QDs to KTaO₃.

regime [68,70]. In general, the quantum confinement shifts the conduction-band edge of smaller CdTe nanocrystals to higher energies, enabling the faster injection of photogenerated electrons into KTaO₃. Therefore the composites containing smaller sized QDs are expected to exhibit the higher photocatalytic activity. In this study this correlation can be observed for TGA-CdTe-KTaO₃ samples containing nanodots refluxed for 0.5, 2, 5 h as well as MPA-CdTe-KTaO₃ composites containing QDs refluxed for 2, 5, 8 h. A possible pathway for the electron transfer from these excited CdTe QDs to KTaO₃ is proposed in Fig. 11b. However, it is worth noting that MPA-CdTe-KTaO₃.0.5 composite exhibited lower photocatalytic activity than TGA-CdTe-KTaO₃.2 sample, probably because of smaller absorption of visible light. Similar results were reported by Wang et al. who developed a PbS QDs-sensitized Cu-TiO₂ photocatalyst of three different sizes of PbS QDs samples (3 nm, 4 nm and 5 nm). Among them, 4 nm PbS QDs-sensitized Cu-TiO₂ showed the highest CO₂ conversion rate due to the combination of optimum absorption of visible spectrum and charge separation properties [71]. In other study, Grigioni et co-workers reported that the 2.8 nm-sized CdSe nanocrystals showed the highest H₂ production rate whereas the 2.5 nm-sized and 3.4 nm-sized CdSe nanocrystals presented lower photocatalytic efficiency toward hydrogen production probably due to fast electron-hole recombination and less negative conduction band energy, respectively [72]. In contrast, Holmes et al. found that H₂ evolution rate increased with decreasing the CdSe QDs size [73].

Furthermore, the presence of bifunctional molecules (such as TGA and MPA) facilitated binding of CdTe QDs to perovskite-like

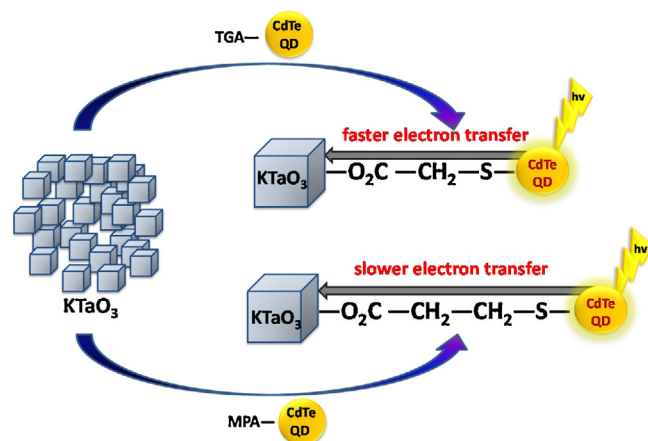


Fig. 12. Scheme of the linker-assisted attachment of CdTe quantum dots to the KTaO₃ semiconductor surface and proposed mechanism based on the effect of linker with various carbon chain length.

KTaO₃ (as shown in Fig. 12) and consequently could cause better interparticle electron transfer between size-quantized CdTe and KTaO₃ semiconductor cubes. The obtained results also may indicate that the type of the bifunctional linker (MPA or TGA) plays a crucial role in determining photocatalytic activity of the capped-CdTe-KTaO₃ composites. The higher photoactivity of all the TGA-capped CdTe-KTaO₃ samples as compared with MPA-capped-CdTe-KTaO₃ composites is probably due to the effect of linker

with varied carbon chain length (TGA: $\text{KTaO}_3-\text{O}_2\text{C}-\text{CH}_2-\text{S}-\text{CdTe}$; MPA: $\text{KTaO}_3-\text{O}_2\text{C}-\text{CH}_2-\text{CH}_2-\text{S}-\text{CdTe}$). The quality of heterojunction between quantum dots and semiconductors substrate could have an influence on the overall photocatalytic performance of composites. Carbon chain length of thioglycolic acid (TGA) smaller than the one of 3-mercaptopropionic acid (MPA) could cause faster electron transfer between CdTe quantum dots and KTaO_3 cubes (Fig. 12.). A similar observation was reported in the case of composites prepared for solar cells applications. Sun et al. [29] fabricated ZnO-based TGA- and MPA-capped CdSe quantum dots sensitized solar cell by low temperature hydrothermal decomposition. It was shown that faster electron transfer and higher power conversion efficiency (PCE) was achieved in ZnO-TGA-CdSe system probably due to shorter chain length of TGA as compared with MPA molecule [29]. In other study, Nevins and co-workers [28] presented functionalization of nanocrystalline TiO_2 films with CdSe quantum dots using three capping groups: cysteinate, 3-mercaptopropionate and mercaptosuccinate for solar cells applications. It was observed that the electronic properties of Cys-capped CdSe NPs differ significantly from those of MP- and MS-capped CdSe NPs [28]. However, our results showed, for the first time, that the type of bifunctional linker has also an importance in regard to photocatalytic activity of obtained materials and therefore may open up a new direction for future research in designing and fabrication of semiconductor photocatalysts decorated with functionalized quantum dots.

4. Conclusions

In summary, for the first time, the CdTe-KTaO₃ composite photocatalysts were successfully synthesized using thioglycolic acid (TGA) or 3-mercaptopropionic acid (MPA) which acted as linker molecules facilitating intimate contact and formation of a stable CdTe-KTaO₃ heterojunction. A longer reflux time of CdTe nanocrystals systematically shifts the absorption and PL peaks to longer wavelengths, which was a clear indication of QDs growth. The incorporation of CdTe QDs into KTaO₃ nanocubes significantly enhanced visible-light absorption properties and improved separation efficiency of photogenerated carriers. Functionalized CdTe-decorated KTaO₃ composites showed greatly improved photocatalytic performance for degradation of toluene in the gas phase under LEDs light irradiation ($\lambda_{\text{max}} = 415 \text{ nm}$) over pristine KTaO₃. Moreover, all TGA-capped CdTe-KTaO₃ composites exhibited higher photocatalytic activity as compared with MPA-capped CdTe-KTaO₃ hybrid which can be related to the shorter chain length of TGA linker as compared with MPA molecule and therefore faster photogenerated electron transfer from CdTe nanocrystals to perovskite-type potassium tantalate. The significant quenching in the fluorescence of CdTe QDs after being deposited on KTaO₃ nanocubes confirmed electron injection from CdTe nanodots into the KTaO₃ conduction band. It was also observed that the photocatalytic activity varies with different-sized CdTe QDs loaded onto KTaO₃ due to the size quantization effect in these nanodots. The highest photocatalytic activity was exhibited by TGA-CdTe-KTaO₃ sample containing 2.04 nm sized CdTe QDs. Our results may provide useful guide for designing and fabrication of efficient photocatalysts based on functionalized quantum dots and wide band gap semiconductors for the environmental purification of organic pollutants.

Acknowledgement

This research was financially supported by National Science Centre, Poland (research grant: "Developing and investigation of a new class of photocatalysts based on colloidal quantum dots and perovskite-type tantalates, zirconates and niobates"; No. 2014/15/N/ST5/03815).

References

- [1] V. Jeyalakshmi, R. Mahalakshmy, K.R. Krishnamurthy, B. Viswanathan, Photocatalytic reduction of carbon dioxide in alkaline medium on La modified sodium tantalate with different co-catalysts under UV-Visible radiation, *Catal. Today* 266 (2016) 160–167.
- [2] B. Bajorowicz, A. Cybula, J.M. Winiarski, T. Klimczuk, A. Zaleska, Surface properties and photocatalytic activity of KTaO₃, CdS, MoS₂ semiconductors and their binary and ternary semiconductor composites, *Molecules* 19 (2014).
- [3] B. Zielińska, E. Mijowska, R.J. Kalenczuk, Synthesis, characterization and photocatalytic properties of lithium tantalate, *Mater. Charact.* 68 (2012) 71–76.
- [4] H. Kato, A. Kudo, Photocatalytic water splitting into H₂ and O₂ over various tantalate photocatalysts, *Catal. Today* 78 (2003) 561–569.
- [5] W. Jiang, X. Jiao, D. Chen, Photocatalytic water splitting of surfactant-free fabricated high surface area NaTaO₃ nanocrystals, *Int. J. Hydrog. Energy* 38 (2013) 12739–12746.
- [6] P. Zhang, J. Zhang, J. Gong, Tantalum-based semiconductors for solar water splitting, *Chem. Soc. Rev.* 43 (2014) 4395–4422.
- [7] H. Yan, X. Wang, M. Yao, X. Yao, Band structure design of semiconductors for enhanced photocatalytic activity: the case of TiO₂, *Progress Nat. Sci.: Mater. Int.* 23 (2013) 402–407.
- [8] K. Iwashina, A. Iwase, A. Kudo, Sensitization of wide band gap photocatalysts to visible light by molten CuCl treatment, *Chem. Sci.* 6 (2015) 687–692.
- [9] X. Ma, Y. Dai, L. Yu, B. Huang, Noble-metal-free plasmonic photocatalyst: hydrogen doped semiconductors, *Sci. Rep.* 4 (2014) 3986.
- [10] H. Chen, L. Wang, Nanostructure sensitization of transition metal oxides for visible-light photocatalysis, *Beilstein J. Nanotechnol.* 5 (2014) 696–710.
- [11] E. Albiter, M.A. Valenzuela, S. Alfaro, G. Valverde-Aguilar, F.M. Martínez-Pallares, Photocatalytic deposition of Ag nanoparticles on TiO₂: Metal precursor effect on the structural and photoactivity properties, *J. Saudi Chem. Soc.* 19 (2015) 563–573.
- [12] F. Odobel, Y. Pellegrin, Recent advances in the sensitization of wide-band-gap nanostructured p-type semiconductors, photovoltaic and photocatalytic applications, *J. Phys. Chem. Lett.* 4 (2013) 2551–2564.
- [13] A.J. Nozik, M.C. Beard, J.M. Luther, M. Law, R.J. Ellingson, J.C. Johnson, Semiconductor quantum dots and quantum dot arrays and applications of multiple exciton generation to third-generation photovoltaic solar cells, *Chem. Rev.* 110 (2010) 6873–6890.
- [14] J. Xia, J. Di, H. Li, H. Xu, H. Li, S. Guo, Ionic liquid-induced strategy for carbon quantum dots/BiOX (X = Br, Cl) hybrid nanosheets with superior visible light-driven photocatalysis, *Appl. Catal. B: Environ.* 181 (2016) 260–269.
- [15] J. Di, J. Xia, M. Ji, L. Xu, S. Yin, Q. Zhang, Z. Chen, H. Li, Carbon quantum dots in situ coupling to bismuth oxyiodide via reactable ionic liquid with enhanced photocatalytic molecular oxygen activation performance, *Carbon* 98 (2016) 613–623.
- [16] F.E. Sarac, C. Yilmaz, F.Y. Acar, U. Unal, CdTe quantum dot sensitized hexanobate nanoscrolls and their photoelectrochemical properties, *RSC Adv.* 2 (2012) 10182–10184.
- [17] S. Wei, R. Zhang, Y. Liu, H. Ding, Y.-L. Zhang, Graphene quantum dots prepared from chemical exfoliation of multiwall carbon nanotubes: an efficient photocatalyst promoter, *Catal. Commun.* 74 (2016) 104–109.
- [18] P. Wang, X. Li, J.L. Fang, D.Z. Li, J. Chen, X.Y. Zhang, Y. Shao, Y.H. He, A facile synthesis of CdSe quantum dots-decorated anatase TiO₂ with exposed {001} facets and its superior photocatalytic activity, *Appl. Catal. B: Environ.* 181 (2016) 838–847.
- [19] J. Di, J. Xia, M. Ji, B. Wang, S. Yin, Y. Huang, Z. Chen, H. Li, New insight of Ag quantum dots with the improved molecular oxygen activation ability for photocatalytic applications, *Appl. Catal. B: Environ.* 188 (2016) 376–387.
- [20] Y. Li, B.-P. Zhang, J.-X. Zhao, Z.-H. Ge, X.-K. Zhao, L. Zou, ZnO/carbon quantum dots heterostructure with enhanced photocatalytic properties, *Appl. Surf. Sci.* 279 (2013) 367–373.
- [21] J. Di, J. Xia, M. Ji, L. Xu, S. Yin, Z. Chen, H. Li, Bidirectional acceleration of carrier separation spatially via N-CQDs/atomically-thin BiOI nanosheets nanojunctions for manipulating active species in a photocatalytic process, *J. Mater. Chem. A* 4 (2016) 5051–5061.
- [22] J. Di, J. Xia, Y. Ge, H. Li, H. Ji, H. Xu, Q. Zhang, H. Li, M. Li, Novel visible-light-driven CQDs/Bi₂WO₆ hybrid materials with enhanced photocatalytic activity toward organic pollutants degradation and mechanism insight, *Appl. Catal. B: Environ.* 168–169 (2015) 51–61.
- [23] W. Cui, W. An, L. Liu, J. Hu, Y. Liang, Novel PbS quantum dots sensitized flower-like BiOBr with enhanced photocatalytic properties under visible light, *Mater. Lett.* 132 (2014) 251–254.
- [24] L. Ge, J. Liu, Synthesis and photocatalytic performance of novel CdS quantum dots sensitized Bi₂WO₆ photocatalysts, *Mater. Lett.* 65 (2011) 1828–1831.
- [25] D.F. Watson, Linker-assisted assembly and interfacial electron-transfer reactivity of quantum dot-substrate architectures, *J. Phys. Chem. Lett.* 1 (2010) 2299–2309.
- [26] S. Qian, C. Wang, W. Liu, Y. Zhu, W. Yao, X. Lu, An enhanced CdS/TiO₂ photocatalyst with high stability and activity: effect of mesoporous substrate and bifunctional linking molecule, *J. Mater. Chem.* 21 (2011) 4945–4952.
- [27] Z. Györi, Z. Kónya, Á. Kukovecz, Visible light activation photocatalytic performance of PbSe quantum dot sensitized TiO₂ Nanowires, *Appl. Catal. B: Environ.* 179 (2015) 583–588.
- [28] J.S. Nevins, K.M. Coughlin, D.F. Watson, Attachment of CdSe nanoparticles to TiO₂ via aqueous linker-assisted assembly: influence of molecular linkers on

electronic properties and interfacial electron transfer, *ACS Appl. Mater. Interfaces* 3 (2011) 4242–4253.

[29] X.W. Sun, J. Chen, J.L. Song, D.W. Zhao, W.Q. Deng, W. Lei, Ligand capping effect for dye solar cells with a CdSe quantum dot sensitized ZnO nanorod photoanode, *Opt. Express* 18 (2010) 1296–1301.

[30] N. Gaponik, A.L. Rogach, Thiol-capped CdTe nanocrystals: progress and perspectives of the related research fields, *Phys. Chem. Chem. Phys.* 12 (2010) 8685–8693.

[31] F.O. Silva, M.S. Carvalho, R. Mendonça, W.A.A. Macedo, K. Balzuweit, P. Reiss, M.A. Schiavon, Effect of surface ligands on the optical properties of aqueous soluble CdTe quantum dots, *Nanoscale Res. Lett.* 7 (2012) 1–10.

[32] Y.-S. Li, F.-L. Jiang, Q. Xiao, R. Li, K. Li, M.-F. Zhang, A.-Q. Zhang, S.-F. Sun, Y. Liu, Enhanced photocatalytic activities of TiO₂ nanocomposites doped with water-soluble mercapto-capped CdTe quantum dots, *Appl. Catal. B: Environ.* 101 (2010) 118–129.

[33] R. Wang, B. Li, L. Dong, F. Zhang, M. Fan, L. Zhou, Photocatalytic activity of CdTe quantum Dots encapsulated in zeolite Y, *Mater. Lett.* 135 (2014) 99–102.

[34] X. Xie, X. Wu, T. Liu, H. Li, Y. Wang, J. Lu, Aqueous synthesis of luminescent cadmium telluride quantum dots using ascorbic acid as the reducing agent, *IET Micro Nano Lett.* 9 (2014) 478–481.

[35] B. Bajorowicz, J. Reszczynska, W. Lisowski, T. Klimczuk, M. Winiarski, M. Sloma, A. Zaleska-Medynska, Perovskite-type KTaO₃-reduced graphene oxide hybrid with improved visible light photocatalytic activity, *RSC Adv.* 5 (2015) 91315–91325.

[36] W.W. Yu, L. Qu, W. Guo, X. Peng, Experimental determination of the extinction coefficient of CdTe, CdSe, and CdS nanocrystals, *Chem. Mater.* 15 (2003) 2854–2860.

[37] A. Ayyaswamy, S. Ganapathy, A. Alsalmi, A. Alghamdi, J. Ramasamy, Structural, optical and photovoltaic properties of co-doped CdTe QDs for quantum dots sensitized solar cells, *Superlattices Microstruct.* 88 (2015) 634–644.

[38] J.-W. Chen, J.-W. Shi, X. Wang, H.-Y. Ai, H.-J. Cui, M.-L. Fu, Hybrid metal oxides quantum dots/TiO₂ block composites: facile synthesis and photocatalysis application, *Powder Technol.* 246 (2013) 108–116.

[39] J. Di, J. Xia, M. Ji, B. Wang, S. Yin, Q. Zhang, Z. Chen, H. Li, Carbon quantum dots modified BiOCl ultrathin nanosheets with enhanced molecular oxygen activation ability for broad spectrum photocatalytic properties and mechanism insight, *ACS Appl. Mater. Interfaces* 7 (2015) 20111–20123.

[40] W. Cui, W. An, L. Liu, J. Hu, Y. Liang, Novel Cu₂O quantum dots coupled flower-like BiOBr for enhanced photocatalytic degradation of organic contaminant, *J. Hazard. Mater.* 280 (2014) 417–427.

[41] J.G. Fisher, A. Benčan, J. Holc, M. Kosec, S. Vernay, D. Rytz, Growth of potassium sodium niobate single crystals by solid state crystal growth, *J. Cryst. Growth* 303 (2007) 487–492.

[42] Y. Hu, H. Gu, Z. Hu, W. Di, Y. Yuan, J. You, W. Cao, Y. Wang, H.L.W. Chan, Controllable hydrothermal synthesis of KTa_{1-x}NbxO₃ nanostructures with various morphologies and their growth mechanisms, *Cryst. Growth Des.* 8 (2008) 832–837.

[43] J. Liu, X. Li, Hydrothermal synthesis of CdTe quantum dots-TiO₂-graphene hybrid, *Phys. Lett. A* 378 (2014) 405–407.

[44] X.-F. Gao, H.-B. Li, W.-T. Sun, Q. Chen, F.-Q. Tang, L.-M. Peng, CdTe quantum dots-sensitized TiO₂ nanotube array photoelectrodes, *J. Phys. Chem. C* 113 (2009) 7531–7535.

[45] R.S. Dibbell, D.G. Youker, D.F. Watson, Excited-state electron transfer from CdS quantum dots to TiO₂ nanoparticles via molecular linkers with phenylene bridges, *J. Phys. Chem. C* 113 (2009) 18643–18651.

[46] L. Hua, H. Han, X. Zhang, Size-dependent electrochemiluminescence behavior of water-soluble CdTe quantum dots and selective sensing of l-cysteine, *Talanta* 77 (2009) 1654–1659.

[47] H. Kumar, R. Srivastava, P.K. Dutta, Highly luminescent chitosan-l-cysteine functionalized CdTe quantum dots film: synthesis and characterization, *Carbohydr. Polym.* 97 (2013) 327–334.

[48] P. Sheng, W. Li, J. Cai, X. Wang, X. Tong, Q. Cai, C.A. Grimes, A novel method for the preparation of a photocorrosion stable core/shell CdTe/CdS quantum dot TiO₂ nanotube array photoelectrode demonstrating an AM 1.5G photoconversion efficiency of 6.12%, *J. Mater. Chem. A* 1 (2013) 7806–7815.

[49] T. Su, H. Jiang, H. Gong, An alternative solid-state method to prepare pyrochlore-free KTaO₃ at low temperature, *J. Solid State Chem.* 184 (2011) 2601–2604.

[50] G.K.L. Goh, S.M. Haile, C.G. Levi, F.F. Lange, Hydrothermal synthesis of perovskite and pyrochlore powders of potassium tantalate, *J. Mater. Res.* 17 (2002) 3168–3176.

[51] Y. Yu, K. Zhang, S. Sun, Effect of ligands on the photoluminescence properties of water-soluble PbS quantum dots, *J. Mol. Struct.* 1031 (2013) 194–200.

[52] G. Sreedhar, A. Sivanantham, S. Venkateshwaran, S.K. Panda, M. Eashwar, Enhanced photoelectrochemical performance of CdSe quantum dot sensitized SrTiO₃, *J. Mater. Chem. A* 3 (2015) 13476–13482.

[53] A. Tkach, P.M. Vilarinho, A. Almeida, Role of initial potassium excess on the properties of potassium tantalate ceramics, *J. Eur. Ceram. Soc.* 31 (2011) 2303–2308.

[54] Y. He, Y. Zhu, N. Wu, Mixed solvents: a key in solvothermal synthesis of KTaO₃, *J. Solid State Chem.* 177 (2004) 2985–2990.

[55] C. Lv, G. Chen, J. Sun, C. Yan, H. Dong, C. Li, One-dimensional Bi2O3 QD-decorated BiVO₄ nanofibers: electrospinning synthesis, phase separation mechanism and enhanced photocatalytic performance, *RSC Adv.* 5 (2015) 3767–3773.

[56] D. Liu, Z. Zheng, C. Wang, Y. Yin, S. Liu, B. Yang, Z. Jiang, CdTe quantum dots encapsulated ZnO nanorods for highly efficient photoelectrochemical degradation of phenols, *J. Phys. Chem. C* 117 (2013) 26529–26537.

[57] H. Borchert, D.V. Talapin, N. Gaponik, C. McGinley, S. Adam, A. Lobo, T. Möller, H. Weller, Relations between the photoluminescence efficiency of CdTe nanocrystals and their surface properties revealed by synchrotron XPS, *J. Phys. Chem. B* 107 (2003) 9662–9668.

[58] U. Winkler, D. Eich, Z.H. Chen, R. Fink, S.K. Kulkarni, E. Umbach, Detailed investigation of CdS nanoparticle surfaces by high-resolution photoelectron spectroscopy, *Chem. Phys. Lett.* 306 (1999) 95–102.

[59] A.V. Naumkin, A. Kraut-Vass, S.W. Gaarenstroom, C.J. Powell, NIST X-ray Photoelectron Spectroscopy Database, NIST Standard Reference Database 20, Version 4.1, 2012 (accessed 25.03.13) <http://srdata.nist.gov/xps/>.

[60] J. Kubacki, A. Molak, M. Rogala, C. Rodenbücher, K. Szot, Metal-insulator transition induced by non-stoichiometry of surface layer and molecular reactions on single crystal KTaO₃, *Surf. Sci.* 606 (2012) 1252–1262.

[61] G.E. McGuire, G.K. Schweitzer, T.A. Carlson, Core electron binding energies in some Group IIIA, VB, and VIB compounds, *Inorg. Chem.* 12 (1973) 2450–2453.

[62] K.H. Reddy, S. Martha, K.M. Parida, Facile fabrication of Bi2O3/Bi-NaTaO₃ photocatalysts for hydrogen generation under visible light irradiation, *RSC Adv.* 2 (2012) 9423–9436.

[63] V.V. Laguta, M.D. Glinchuk, I.P. Bykov, A. Cremona, P. Galinetto, E. Giulotto, L. Jastrabik, J. Rosa, Light-induced defects in KTaO₃, *J. Appl. Phys.* 93 (2003) 6056–6064.

[64] S. Jin, H.-J. Son, O.K. Farha, G.P. Wiederrecht, J.T. Hupp, Energy transfer from quantum dots to metal–organic frameworks for enhanced light harvesting, *J. Am. Chem. Soc.* 135 (2013) 955–958.

[65] U. Soni, P. Tripathy, S. Sapra, Photocatalysis from fluorescence-quenched CdSe/Au nanoheterostructures: a size-dependent study, *J. Phys. Chem. Lett.* 5 (2014) 1909–1916.

[66] A. Cybula, G. Nowaczyk, M. Jarek, A. Zaleska, Preparation and characterization of Au/Pd modified-tio 2 photocatalysts for phenol and toluene degradation under visible light—the effect of calcination temperature, *J. Nanomater.* 2014 (2014) 2.

[67] M. Nischk, P. Mazierski, M. Gazda, A. Zaleska, Ordered TiO₂ nanotubes: the effect of preparation parameters on the photocatalytic activity in air purification process, *Appl. Catal. B: Environ.* 144 (2014) 674–685.

[68] P. Wang, D. Li, J. Chen, X. Zhang, J. Xian, X. Yang, X. Zheng, X. Li, Y. Shao, A novel and green method to synthesize CdSe quantum dots-modified TiO₂ and its enhanced visible light photocatalytic activity, *Appl. Catal. B: Environ.* 160–161 (2014) 217–226.

[69] A. Kudo, Y. Miseki, Heterogeneous photocatalyst materials for water splitting, *Chem. Soc. Rev.* 38 (2009) 253–278.

[70] Z. Lu, C.X. Guo, H.B. Yang, Y. Qiao, J. Guo, C.M. Li, One-step aqueous synthesis of graphene-CdTe quantum dot-composed nanosheet and its enhanced photoresponses, *J. Colloid Interface Sci.* 353 (2011) 588–592.

[71] C. Wang, R.L. Thompson, P. Ohodnicki, J. Baltrus, C. Matranga, Size-dependent photocatalytic reduction of CO₂ with PbS quantum dot sensitized TiO₂ heterostructured photocatalysts, *J. Mater. Chem.* 21 (2011) 13452–13457.

[72] I. Grigioni, M. Bernareggi, G. Sinibaldi, M.V. Dozzi, E. Sellì, Size-dependent performance of CdSe quantum dots in the photocatalytic evolution of hydrogen under visible light irradiation, *Appl. Catal. A: Gen.* 518 (2016) 176–180.

[73] M.A. Holmes, T.K. Townsend, F.E. Osterloh, Quantum confinement controlled photocatalytic water splitting by suspended CdSe nanocrystals, *Chem. Commun.* 48 (2012) 371–373.